SCIENCE CHINA
Technological Sciences

• Research Paper •

*** 2010 Vol.** No.: **–**
doi:

# Aerodynamic Noise Analysis of Large Horizontal Axis Wind Turbines Considering Fluid-Structure Interaction

Ho Geon Kim[1], Seung Hoon Lee[1], Eun Kuk Son[1], Seung Min Lee[1], Soo Gab Lee[2*]

[1] *Department of Mechanical and Aerospace Engineering, Seoul National University, Seoul, Korea*
[2] *Institute of Advanced Aerospace Technology, Department of Mechanical and Aerospace Engineering, Seoul National University, Seoul, Korea*

Received November 17, 2010; accepted XX, XX; published online XX, XX

Aerodynamic Noise is one of the most serious barriers in wind energy development. To develop noise reduction technologies and assess wind turbine noise, more precise noise prediction is needed. Especially, an important factor that should be considered for calculating noise accurately is the blade flexibility. The numerical tool, WINFAS, includes fluid-structure interaction, consists of three parts. The Unsteady Vortex Lattice Method is used for aerodynamic part and the Nonlinear Composite Beam Theory is applied for structural part. In third part of WINFAS, to analyze aerodynamic noise, semi-empirical formula of airfoil self noise and Lowson's formula of turbulence ingestion noise are used. In this study, using this numerical method, the noise source position and strength change due to blade flexibility was examined. This research shows that elastic blades decrease broadband noise because pitching motion reduces angle of attack.

**aerodynamic noise, nonlinear composite beam theory, nonlinear vortex correction method, fluid-structure interaction**

## 1 Introduction

Wind energy industry has been rapidly increased around the world as a practical solution for Low-Carbon Green Growth. However, social and environmental problems such as landscape damage, shadow flicker, noise, electromagnetic interference et al. have hindered for wind energy development. Among them, the issue on noise has become the biggest problem [1].

Two kinds of approaches are mainly needed to resolve wind turbine noise. One is that reduce the generated noise [2] and the other is that determined the extent of noise impact and then make a post-compensation or reduce the pre-damage during the wind farm construction. To do this, we need a proper noise analysis and propagation method. In a recent, the size of wind turbine becomes larger. For example, in 1960s, the diameter of wind turbine is only 40m; however, nowadays, it is over 120m [3-4]. Since these large wind turbines are more flexible, aeroelastic deformation has to be considered for wind turbine system analysis and its design [5]. Besides, process of the noise analysis is until now assumed that the blade is rigid but the necessity considering the blade flexibility for aerodynamic noise analysis is arisen. The purpose of this study is investigation into the effects of the deformation of large wind turbine blade to the aerodynamic noise.

To view the effects of the blade flexibility on the aerodynamic noise, three kinds of methods are used. In the part of the aerodynamic analysis, the Nonlinear Vortex Correction Method [6], based on the Unsteady Vortex Lattice Method, designed for the calculation beyond the stall region is used and the Nonlinear Composite Beam Theory developed by D. H. Hodges [7-8] is used for the structure analysis. Finally, Turbulent Ingestion (TI) noise [9] and Turbulent Boundary Layer Trailing Edge [10] noise analysis are performed with information on the blade deformation and the flow filed.

*Corresponding author (email: solee@snu.ac.kr)

## 2 Numerical Method

Figure 1 shows schematic diagram of wind turbine blade aerodynamic noise analysis considering Fluid-Structure Interaction (FSI). Numerical method is consists of three parts: aerodynamic part, structural part, and aeroacoustic part. The Nonlinear Vortex Correction Method (NVCM) that is based on the Unsteady Vortex Lattice Method (UVLM) and is able to calculate stall region is used for Aerodynamic part. In structural dynamic part, the Nonlinear Composite Beam Theory (NCBT) that D.H. Hodges derived is used. In order to improve convergence of aerodynamic and structural solution, structural code is converged in vacuum first, and loosely coupled analysis is computed with slow starting during 1 revolution. After pre-convergence procedure, full load condition is applied to calculate FSI. In this research, total 10 revolutions are performed with full load.

After FSI calculation, aerodynamic noise analysis is performed using blade deformation, effective angle of attack, and onset velocity on each blade section. Because main sources of wind turbine aerodynamic noise are Turbulent Ingestion (TI) and Turbulent Boundary Layer Trailing Edge (TBLTE) noise, we calculated two noise sources in this study.

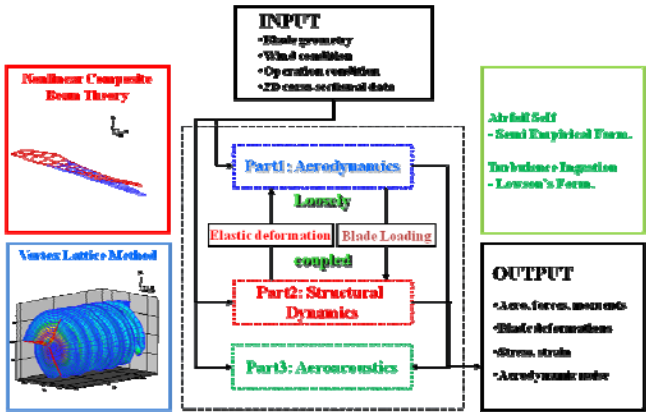


**Figure 1** The Schematic procedure of wind turbine aerodynamic noise analysis considering**.**

### 2.1 Nonlinear Vortex Correction Method

The UVLM based on potential flow cannot calculate thickness and viscous effects. Therefore, a two-dimensional table should be used [11-12] to consider these effects inherently. However, an incorrect angle of attack and aerodynamic coefficients are calculated from a two-dimensional table because the UVLM evaluates the bound circulations on the lifting surface without regard to thickness and viscous effects. That is corrected by matching up the sectional lift from the UVLM with that from 2-dimensional table look-up [6].

The NVCM is summarized as follows:

$$\begin{aligned}&\textit{Initial stage : If } F = dL_{UVLM} - dL_{table\ \ look-up} \neq 0\\ &\textit{then : } \Gamma_{initial} \pm \Delta\Gamma \rightarrow \Gamma_{mod\,ified}\\ &\textit{Final stage : If } F \rightarrow 0, \textit{then use } \Gamma_{mod\,ified}\end{aligned}$$

where $dL_{UVLM}$ and $dL_{table\ look-up}$ indicate sectional lift from the UVLM and the table look-up procedure, respectively; $F$ is the difference between these two values; and $\Gamma$ indicates the bound vortex strength of the blade spanwise section. Using the unsteady Bernoulli equation and the pressure difference, $dL_{UVLM}$ is computed from the UVLM. In this research, to consider 3-dimensional stall delay AirfoilPrep [13] was used. The local effective angle of attack and the Reynolds number are calculated using the UVLM. Then, $dL_{table\ look-up}$, sectional drag and sectional pitching moment were obtained by interpolating from the airfoil data table according to the calculated effective angle of attack and the Reynolds number.

If $F$ is not zero, $F$ is modified by matching process between $dL_{UVLM}$ and $dL_{table\ look-up}$ using addition or subtraction of $\Delta\Gamma$ which is equal value in one span wise section.

However, in this process, a problem for determination of the bound vortex strength by matching arises from nonlinearity between the bound vortex strength and the angle of attack for not only independent strips but also neighboring blade strips. For this reason, this process has to be represented by a nonlinear system of equations:

$$\begin{aligned}F_1(\vec{x}) &= (dL_{UVLM})_1 - (dL_{table\ look\text{-}up})_1\\ F_2(\vec{x}) &= (dL_{UVLM})_2 - (dL_{table\ look\text{-}up})_2 \quad (1)\\ &\vdots \qquad\quad \vdots \qquad\quad \vdots\\ F_n(\vec{x}) &= (dL_{UVLM})_n - (dL_{table\ look\text{-}up})_n\end{aligned}$$

where $x_1 = \Delta\Gamma_1$ , $x_n = \Delta\Gamma_n$ and $\vec{x} = (x_1, x_2, \cdots, x_n)$. Subscript n is the total number of blade spanwise sections. The vector form of eq. (1) is given by

$$\vec{F}(\vec{x}) = 0 \quad (2).$$

Eq. (2) can be solved by applying by a sophisticated Newton-Raphson iterative method with a rapid local convergence algorithm and a globally convergent strategy [14].

The wake shed from the trailing edge is described using a vortex ring to predict wake convection. At each time step, the free wake moves with the total velocity.

## 2.2 Nonlinear Composite Beam Theory

Rotating beam coordinate systems are shown in figure 2. Coordinate 'a' is a global frame, with its axes labeled $a_1$, $a_2$, and $a_3$ is rotating with the rotor. Undeformed blade coordinate is 'b' frame. Blade's deformed frame is named 'B' with its axes are $B_1$, $B_2$, and $B_3$.

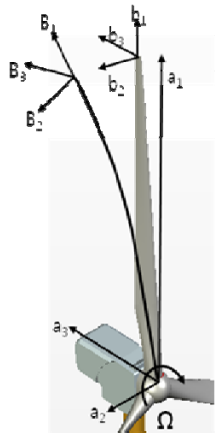


**Figure 2** The Coordinates system for dynamics of moving beam. 'a' frame is global coordinates rotating with rotor. 'b' frame is undeformed blade coordinate. 'B' is blade's deformed frame.

An arbitrary vector $U$ that is in 'a' frame can be expressed by its components in 'B' or 'b' frame using the transformation matrices such as below

$$U_B = C^{Ba}U_a\,, \quad U_b = C^{ba}U_a \tag{3}$$

where $C^{Ba}$ is the transformation matrix from 'a' to 'B', and $C^{ba}$ is that from 'a' to 'b'.

Mixed form of the variational equation is used for the blade structure modeling. Hamilton's principle is used for the formulation derivation and it is written as

$$\int_{t_1}^{t_2}\int_0^l \left[\delta(K-U)+\overline{\delta W}\right]dx_1 dt = \overline{\delta A} \tag{4}$$

where $t_1$ and $t_2$ are arbitrary fixed times, $l$ means length of beam. $K$ and U are the kinetic and potential energy per unit length. $\overline{\delta A}$ is the virtual action at the ends of beam and time interval. $\overline{\delta W}$ is the virtual work of applied loads per unit length. Partial derivatives of $U$ and $K$ with respect to $\gamma$, $\kappa$, $V_B$ and $\Omega_B$ are the internal force and moment vectors $F_B$ and $M_B$, and linear and angular momentum vectors $P_B$ and $H_B$ are defined as

$$F_B = \left(\frac{\partial U}{\partial \gamma}\right)^T, M_B = \left(\frac{\partial U}{\partial \kappa}\right)^T \tag{5}$$
$$P_B = \left(\frac{\partial K}{\partial V_B}\right)^T, H_B = \left(\frac{\partial K}{\partial \Omega_B}\right)^T$$

where $\gamma$ and $\kappa$ are force and momentum strain and $V_B$ and $\Omega_B$ are linear and angular velocity. The first component of $F_B$ is axial force ($B_1$ axis, outward direction from root to tip) and the second and third term are shear force. As same convention of $F_B$, torsional moment is the first term of $M_B$ and the second and third term of $M_B$ mean bending moment (more details in ref. [8]).

For mixed variational form, Lagrange's multipliers are used and the complete variational formulation can be derived in 'a' frame based on geometrically exact equation.

$$\int_{t_1}^{t_2}\delta\Pi_a dt = 0$$

$$\begin{aligned}\delta\Pi_a = \int_{t_1}^{t_2}\Big\{&\delta u_a' C^T C^{ab} F_B + \delta u_a^T\left[\left(C^T C^{ab} P_B\right)^{\bullet} + \tilde{\omega}_a C^T C^{ab} P_B\right]\\
&+ \overline{\delta\psi}_a' C^T C^{ab} M_B - \overline{\delta\psi}_a C^T C^{ab}\left(\tilde{e}_1+\tilde{\gamma}\right)F_B\\
&+ \overline{\delta\psi}_a^T\left[\left(C^T C^{ab} H_B\right)^{\bullet} + \tilde{\omega}_a C^T C^{ab} H_B + C^T C^{ab}\tilde{V}_B P_B\right]\\
&- \overline{\delta F}_a^T\left[C^T C^{ab}\left(e_1+\gamma\right) - C^{ab}e_1\right] - \overline{\delta F}_a'^T u_a\\
&- \overline{\delta M}_a^T\left(\Delta + \frac{\tilde{\theta}}{2} + \frac{\theta\theta^T}{4}\right)C^{ab}\kappa - \overline{\delta M}_a' u_a\\
&+ \overline{\delta P}_a^T\left(C^T C^{ab} V_B - v_a - \tilde{\omega}_a u_a - \overline{\delta P}_a^T \dot{u}_a\right)\\
&+ \overline{\delta H}_a^T\left(\Delta - \frac{\tilde{\theta}}{2} + \frac{\theta\theta^T}{4}\right)\left(C^T C^{ab}\Omega_B - \omega_a\right)\\
&- \overline{\delta H}_a^T\dot{\theta} - \delta u_a^T f_a - \overline{\delta\psi}_a^T m_a\Big\}dx_1\\
&- \left(\delta u_a^T\hat{F}_a + \overline{\delta\psi}_a^T\hat{M}_a - \overline{\delta F}_a^T\hat{u}_a - \overline{\delta M}_a^T\hat{\theta}_a\right)\Big|_0^l\end{aligned} \tag{6}$$

where $f_a$ and $m_a$ are aerodynamic force and moment vector. $\delta u_a^T f_a - \overline{\delta\psi}_a^T$ is the virtual work of aerodynamic load per unit length. $\hat{F}_a$, $\hat{M}_a$, $\hat{u}_a$ and $\hat{\theta}_a$ are boundary conditions. For wind turbine case, $\hat{F}_a$, $\hat{M}_a$ of blade tip are zero and $\hat{u}_a$ and $\hat{\theta}_a$ of blade root are zero (see more details in ref. [8]).

For finite element discretization, the blade is divided into N elements, and eq. (6) can be rewritten as

$$\int_{t_1}^{t_2}\sum_{i=1}^{N}\delta\Pi_i dt = 0 \tag{7}$$

where $i$ is an $i$-th element with length $dl$ and $\delta\Pi_i$ is the corresponding spatial integration over the $i$-th of eq. (6). Because eq. (7) derived by mixed variational formulation,

simple shape functions can be used. Substitution and interpolation such as eq. (8) are accomplished on each element.

$$
\begin{aligned}
&x = x_i + \xi \Delta l_i, \quad dx = \Delta l_i d\xi, \quad (\ )' = \frac{1}{\Delta l_i}\frac{d}{d\xi}(\ ) \\
&\delta u_a = \delta u_i(1-\xi), + \delta u_{i+1}\xi, \quad u_a = u_i \\
&\overline{\delta\psi}_a = \overline{\delta\psi}_i(1-\xi), + \overline{\delta\psi}_{i+1}\xi, \quad \theta = \theta_i \\
&\overline{\delta F_a} = \overline{\delta F_i}(1-\xi), + \overline{\delta F}_{i+1}\xi, \quad F_B = F_i \\
&\overline{\delta M_a} = \overline{\delta M_i}(1-\xi), + \overline{\delta M}_{i+1}\xi, \quad M_B = M_i \\
&\overline{\delta P_a} = \overline{\delta P_i}, \quad P_B = P_i \\
&\overline{\delta H_a} = \overline{\delta H_i}, \quad H_B = P_i
\end{aligned}
\tag{8}
$$

where $\xi$ is value from 0 to 1.

Using eqn. (6)~(8), discretization can be accomplished on the structural and aerodynamic part, then the resulting equations can be simplified as follows

$$F_S(X, \dot{X}) - F_L = 0 \tag{9}$$

where $F_S$ is the structural operator, $F_L$ is the aerodynamic operator, and $X$ is the unknown vector. A second-order backward Euler method is applied for time integration, and one can get a nonlinear algebraic equation at $n$-th time step.

$$F_S(X^n) - F_L = 0 \tag{10}$$

Eq. (10) can be solved using Newton's method. The solutions of eq. (10) are displacement, stress and strain at each time step.

## 2.3 Aerodynamic Noise Model

Effective angles of attack, onset velocities and deformations which are calculated using FSI are used for analysis of wind turbine aerodynamic noise. In this study, Turbulent Ingestion noise(TI) [9] is predicted using Lowson's model and Semi-Empirical formula [10] is applied for Turbulent Boundary Layer Trailing Edge noise(TBL-TE) because TI and TBL-TE noise are main sources of wind turbine aerodynamic noise. Boundary layer displacement thickness data that is needed to calculate TBL-TE noise are tabulated and categorized according to Reynolds Number, angle of attack, onset velocity and r/R using Xfoil [15].

TI noise is generated by the interaction of atmospheric turbulence with rotor blade because of pressure fluctuation. High and low frequency TI noise can be analyzed by eq. (11) that Lowson [9] adopted the model of Amiet [16]

$$
\begin{aligned}
&SPL_{TIN}^{H} = 10\log_{10}\left[\rho^2 c_0^2 L \frac{\Delta l}{r^2} M^3 I^3 k^3 (1+k^2)^{-7/3}\right] + 58.4 \\
&SPL_{TIN}^{L} = SPL_{TIN}^{H} + 10\log_{10}\left(\frac{K_{lfc}}{1+K_{lfc}}\right) \\
&k = \pi f c / V, \quad \beta^2 = 1 - M^2, \quad K_{lfc} = 10 S^2 M \frac{k^2}{\beta^2} \\
&S^2 = \left(\frac{2\pi k}{\beta^2} + \frac{1}{1+2.4k/\beta^2}\right)
\end{aligned}
\tag{11}
$$

where $K_{lfc}$ is the low frequency correction factor, $\rho$ is density of air, $M$ is Mach number, $V$ is onset velocity, $c_0$ is speed of sound, $I$ indicates the turbulence intensity and $L$ indicates the length scale of turbulence.

A boundary layer develops on the blade surface. Transition from laminar to turbulent flow occurs and induces a fluctuating pressure field. When turbulent eddies meet a sharp edge like training edge, they become more efficient. TBL-TE noise can be predicted by below equations (details in ref. [10]).

$$
\begin{aligned}
&SPL_{TBLTE} = 10\log_{10}\left[10^{SPL_s/10} + 10^{SPL_p/10} + 10^{SPL_\alpha/10}\right] \\
&SPL_s = 10\log_{10}\left(\frac{\delta_s^* M^5 D_h \Delta l}{r^2}\right) + G_A\left(\frac{St_s}{St_1}\right) + W_1 - 3 \\
&SPL_p = 10\log_{10}\left(\frac{\delta_p^* M^5 D_h \Delta l}{r^2}\right) + G_A\left(\frac{St_p}{St_1}\right) + W_1 - 3 + \Delta W \\
&SPL_\alpha = 10\log_{10}\left(\frac{\delta_s^* M^5 D_h \Delta l}{r^2}\right) + G_B\left(\frac{St_s}{St_2}\right) + K_2
\end{aligned}
\tag{12}
$$

# 3 Results

## 3.1 Validation

Unfortunately, there is not proper validation data that one can consider aerodynamics, structure and aeroacousics together. Therefore, validation of three parts of WINFAS was performed separately.

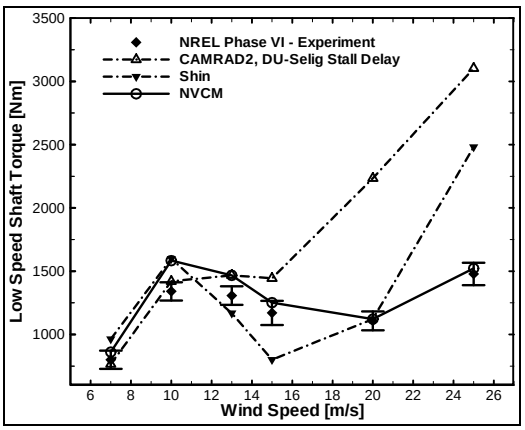


**Figure 3** The low speed shaft torque comparison with NREL Phase VI experiment [17-19]. Shin used vortex lattice method based on free wake without post stall consideration [20]. CMRAD2 is based on Lifting Line Method [21].

The comparison of low speed shaft torque between the NREL Phase-VI experiments [17-19] is shown in Figure 3. The results calculated by the NVCM of WINFAS are in good agreement with experiments.

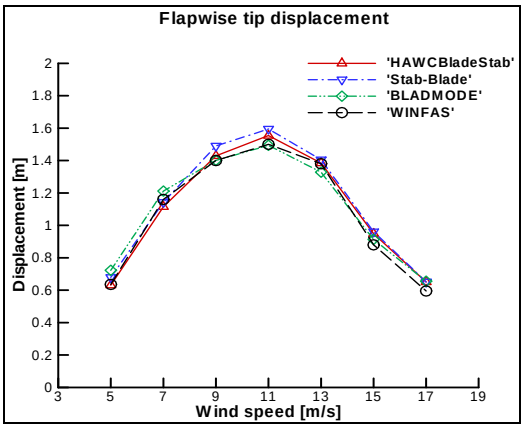


**Figure 4** The comparison of flapwise blade tip deformation of RB 70 [22]. HAWCBladeStab is program of Risø for the aeroelastic stability of blade vibrations. Stab-Blade is program of CRES for the aeroelastic stability of blade vibrations. BLDMODE is program of ECN for the rotor blade eigenmode analysis

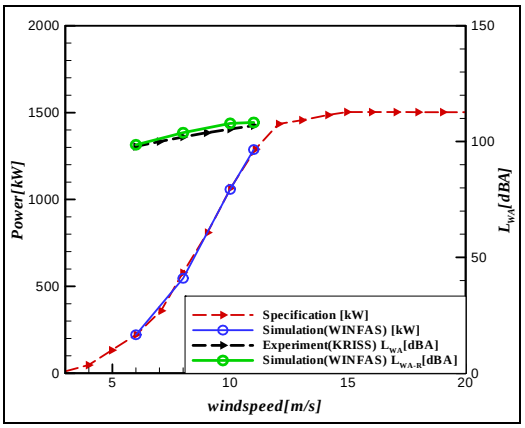


**Figure 5** The power and sound power level of NM-72 per wind speed. Specification means the power curve provided by NEG-Micon. Noise measurement was performed by KRISS detailed in ref. [23].

In order to validate structural part, flapwise tip displacement of WINFAS was compared with that of other numerical tools. RB 70 rotor blade [22] that radius is 35.2m and rated power is 1.5MW was used for validation. As seen Figure 4. WINFAS' results are good consistent with other numerical tools.

By comparison with the noise measurements [23], verification of noise prediction part of WINFAS was performed as seen Figure 5 and 6. Figure 5 indicates good agreement between sound power level ($L_{WA}$) of experiments and that of simulation. Though by spectrum comparison in Figure 6, differences are observed in some frequency regions, it can be seen good agreement generally. Note that NM-72 is active stall control type and several peaks of measurement spectrum can come from mechanical part such as gearbox.

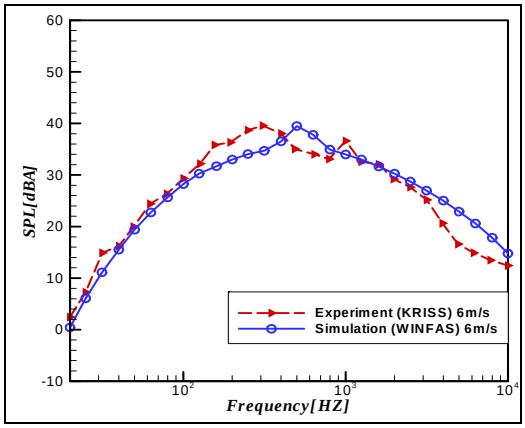


**Figure 6** The One-third octave band spectrum in 6m/s. Noise measurement was performed by KRISS detailed in [23].

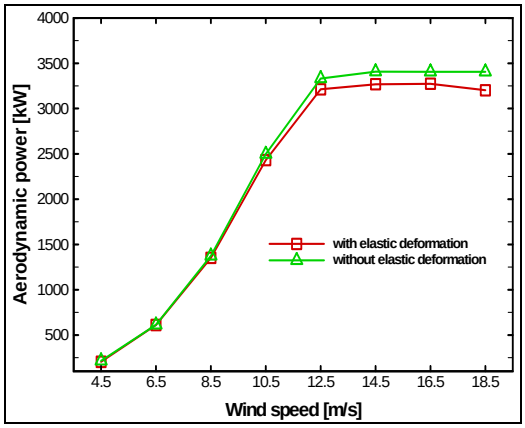


**Figure 7** The aerodynamic power considering elastic deformation. The normalized differences between power of case without deformation and that of case with deformation are about 5% over wind speed of 10.5 m/s.

## 3.2 Noise calculation

The rotor of 3MW wind turbine system which has 3 blades whose radius is 45.8m and rated wind speed is

12.5m/s with 15.7 rated rpm was used for the aerodynamic noise calculation. Airfoils the blade consists of are DU series whose thickness is from 40% to 20% and NACA64-618 in the tip region. The blade was divided up into 15 vortex lattices along the radial directions and two vortex lattices along the chordwise directions for simulation. A azimuthal step size is 6°.

The Aerodynamic power difference which is normalized by the power with consideration FSI is about 5% over 10.5m/s. Blade deformation makes effective angle of attack and onset velocity change. Especially blade pitching down due to blade flexibility would be the biggest effect on angle of attack decrease. As a result, its decrease reduces aerodynamic load as seen Figure 7.

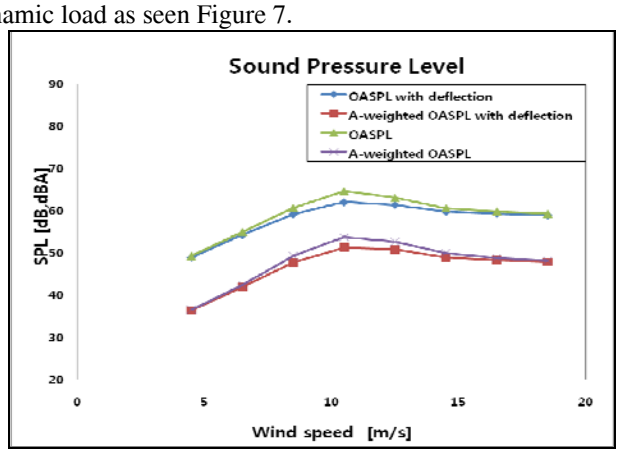


**Figure 8** The sound pressure level of various wind speed cases in uniform flow. In the rated wind speed, 11.5m/s and 10.5m/s, the SPL difference between the case of considering deflection and that of not considering deflection is about 2~1.5dB.

Figure 8 describes the difference between SPL of flexible blade and that of rigid blade. In contrast to the tendency of aerodynamic power due to blade flexibility, there is no significant noise level difference which is caused by blade deformation as wind speed is over 14.5m/s. The rotor rotational speed of most modern large wind turbines reaches rated RPM as wind speed is below just 1~2m/s of rated speed. Moreover, pitch control keeps constant electric power level operates when wind speed is over rated wind speed.

Therefore, because wind turbine blade operates in the condition of low angle of attack through the whole blade as wind speed is over 12.5m/s, angle of attack difference due to pitching down does not significantly affect on aerodynamic noise change. Moreover, because the velocity due to rotation that is a component of total onset velocity on each section is constant over rated wind speed, TBL-TE noise does not change seriously.

Figure 9 and 10 show the frequency spectrum of TBLTE noise considering FSI in 10.5m/s and 18.5m/s. As seen in Figure 10, TBLTE-α and TBLTE-S noise increase because of blade deflection in wind speed of 10.5m/s. When wind speed is 18.5m/s, the angle of attack reduced by tensional deflection does not change TBLTE noise significantly as mentioned above, because the tip and mid region of blade have low angle of attack. SPL footprint is shown in Figure 11 and 10 on the flat terrain. Sound power level which was predicted in rigid blade condition is higher than that calculated in flexible blade condition near wind turbine position, (x,y)=(0,0).

## 4 Conclusions

This paper describes the effects of blade flexibility on aerodynamic noise. For considering Fluid-Structure Interaction, the NVCM was used for aerodynamic analysis and blade structural dynamics was modeled in the Nonlinear Composite Beam Theory. Finally, the flow data such as

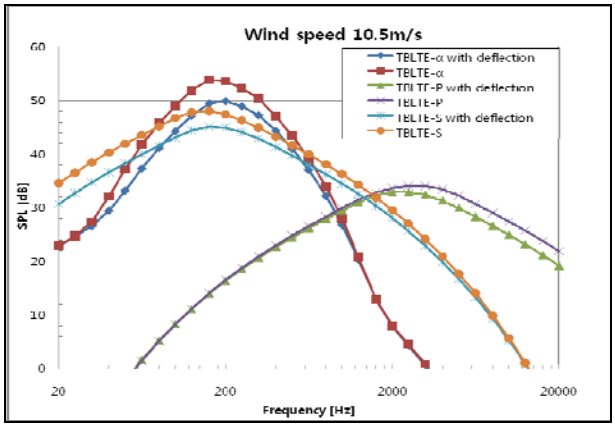


**Figure 9** The frequency spectrum of TBLTE noise in wind speed of 10.5m/s. TBLTE-P is turbulent boundary layer pressure side noise. TBLTE-S indicates turbulent boundary layer suction side noise. TBLTE-α means separated flow noise.

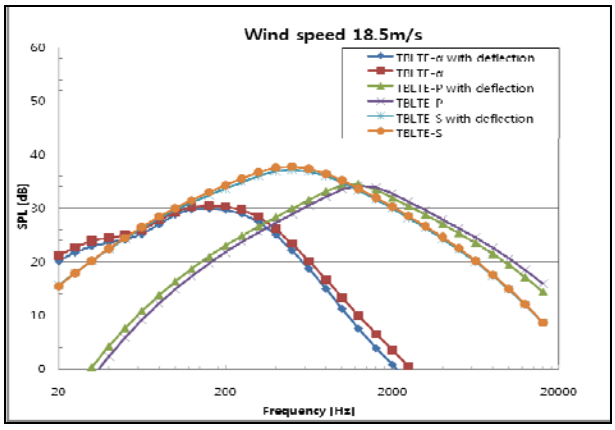


**Figure 10** The frequency spectrum of TBLTE noise in wind speed of 18.5m/s.

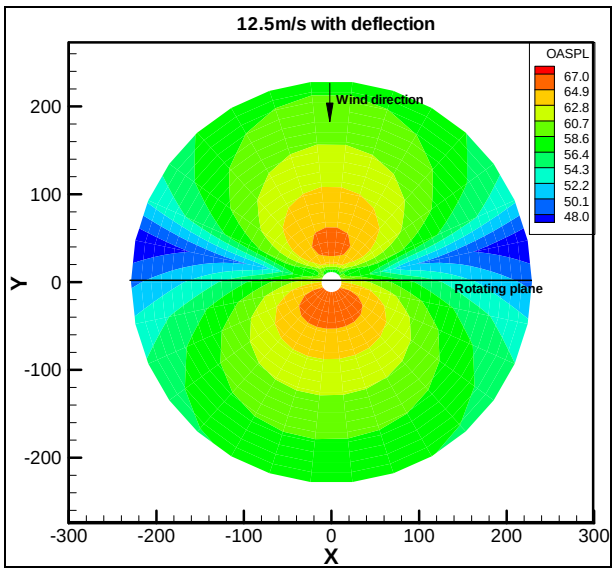


**Figure 11** The footprint of overall sound pressure level with deflection in wind speed of 12.5m/s.

effective angle of attack, blade deformed geometry and onset velocity, calculated by the numerical method with or without FSI, were used for prediction of aerodynamic noise, TBLTE noise. In 8~12m/s of uniform flow, sound pressure level of considering blade deflection case was about 1.5~2.5 dB low compare to rigid blade. When wind speed is over 12m/s, rated wind speed, noise changes caused by blade flexibility were not significant because wind turbine blade operates low angles of attack range on mid and tip region of the blade due to pitch control that modern large wind turbines have. In other words, the reason is that angle of attack changes in the condition of low angle of attack, around 0˚, produce smaller variations than that in the condition of high angle of attack, around 5˚.

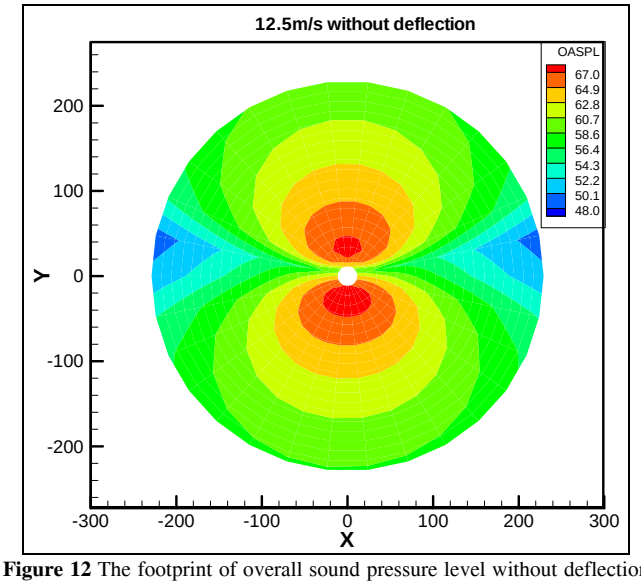


**Figure 12** The footprint of overall sound pressure level without deflection in wind speed of 12.5m/s.

In the aspect of noise assessment, the amount of time it takes to predict the noise produced by modern large wind turbine considering FSI is too long. Therefore, for the wind speeds in which blade flexibility affects on aerodynamic noise, it is proper approach to correct over predicted sound pressure level that rigid blade generates.

This research was limited to steady uniform flow condition and pitch controlled and variable speed wind turbine. What remains to be determined by future research is studies about the blade flexibility effect on noise generated by types of wind turbine system, for example individual pitch control and stall control, and unsteady wind condition, the time variance of wind velocity.

*This work was supported by the Human Resources Development and the New and Renewable Energy of the Korea Institute of Energy Technology Evaluation and Planning (KETEP) grant funded by the Korea government Ministry of Knowledge Economy (No. 20094020100060 & No. 2009T1001 00231)*

1 Johansson L. Summary of IEA Topical Expert meeting on Noise Immission, 2000
2 Kim T H, Lee S M, Kim H G, et al. Design of Low Noise Airfoil with High Aerodynamic Performance for Use on Small Wind Turbines. Sci China Tech Sci, 2010, 53: 75-79
3 Harrison R, Hau E, Snel H. Large Wind Turbine: Design and Economics. John Wiley & Sons. Ltd, West Sussex, England, 2000 : 1-26
4 EWEA. WIND ENERGY – THE FACTS PART I: TECHNOLOGY. European Wind Energy Association, 2009 : 72-79
5 Hansen M O L, Sørensen J N, Voutsinas S, et al. State of the art in wind turbine aerodynamics and aeroelasticity. Progress in Aerospace Sciences , 2006, 42: 285-330
6 Kim H G, Lee S M, Lee S G. Numerical Analysis on the Aerodynamics of HAWTs using Nonlinear Vortex Strength Correction. Curr. Appl. Phys., 2010, 10: s311-s315
7 Hodges D H, Yu W. A Rigorous, Engineer-friendly Approach for Modelling Realistic, Composite Rotor Blades. Wind Energ. 2007, 10: 179-193
8 Shang X, Hodges D H, Peters D A. Aeroelastic Stability of Composite Hingless Rotors in Hover with Finite-State Unsteady Aerodynamics. J American Helicopter Society. 1999, 44: 206-221
9 Lowson M V. Assessment and Prediction Model for Wind Turbine Noise: Basic Aerodynamic and Acoustic Models. Flow Solution Report, 1993
10 Brooks F T, Pope D S, Marcolini M A. Airfoil Self-noise and Prediction. NASA Reference Publication, 1989, 1218: 1-145
11 Prandtl L, Tietjens O G. Applied hydro-and aeromechanics. DOVER, New York, USA, 1934
12 van Garrel A. Development of windturbine aerodynamics simulation module. ECN-C--03-079, 2003
13 NWTC Design Codes (AirfoilPrep by Dr. Craig Hansen), *http://wind.nrel.gov/designcodes/preprocessors/airfoilprep/*. Last modified 16-January-2007, accessed on: 16-January-2007
14 Press W H, Teukolsky S A, Vetterling W T, et al. Numerical recipes in fortran: the art of scientific computing. 2nd edition, Cambridge University Press, Cambridge, England, 1992, 372-386.
15 Drela M. An Analysis and Design System for Low Reynolds Number Aifoils. Conference on Low Reynolds Number Aerodynamics, 1989
16 Amiet R K. Acoustic Radiation from an Airfoil in a Turbulent Stream. J Sound and Vibration, 1975, 41: 407-420
17 Hand M M, Simms D A. Fingersh L J, et al. Unsteady aerodynamics experiment phase VI: Wind tunnel test configurations and available data

campaigns. NREL/TP-500-29955, 2001
18 Simms D A, Schreck S, Hand M M, et al. Plans for testing the NREL unsteady aerodynamics experiment 10-m diameter HAWT in the NASA Ames wind tunnel. NREL/TP-500-27599,1999
19 Simms D A, Schreck S, Hand M M, et al. Unsteady aerodynamics experiment in the NASA-Ames wind tunnel: comparison of predictions to measurements. NREL/TP-500-29494, 2001
20 Shin H. Numerical and experimental analysis of performance, aerodynamic load and noise on HAWT blade. Ph.D. Dissertation, Dept. of Aerospace Engineering, Seoul National University, 2005
21 Duque E P N, Burklund M D, Johnson W. Navier-Stokes and Comprehensive Analysis Performance Predictions of the NREL Phase VI Experiment. AIAA Paper No. 2003-0355, ASME Wind Energy Symposium, 2003, 1-19.
22 Lindenburg C. Structural Pitch for a Pitch-to-Vane Controlled Wind Turbine Rotor. ECN-C--03-087, 2004
23 Lee S, Cheong C. Experimental Investigation into Infrasound and Low-frequency Noise Radiation Characteristics from Large Wind Turbines. The Korean Society for Noise and Vibration Engineering, 07A-53-03, 2007